In-Situ Growth of a Feather-like MnO_2 Nanostructure on Carbon Paper for High-Performance Rechargeable Sodium-Ion Batteries

Huan Li, [a] Anmin Liu, [b] Shuai Zhao, [c] Zhanglin Guo, [a] Nannan Wang, [a] and Tingli Ma*[a]

Abstract: Recently, sodium-ion batteries have attracted great attention due to the rich resource and low cost. In the present work, a feather-like MnO_2 nanostructure was prepared directly on a carbon paper using a rapid and simple hydrothermal route for the first time. The formation mechanism was proposed by investigating the intermediate products during the reaction. When applied as anode for sodium-ion battery, the feather-like MnO_2 nanostructure on carbon paper exhibited a high discharge capacity, good rate reversibility and long-term cycling stability. High specific capacity of ~300 mAh g^{-1} could be obtained even after cycling for 400 times with a current density of 0.1 A g^{-1}. Furthermore, the Na^+ storage mechanism of MnO_2 on carbon paper in the sodium-ion battery was also investigated in this work. Such high performance can be attributed to the porous structure of the substrate and high specific surface area of the feather-like nanostructure.

Introduction

Lithium ion batteries (LIBs) have been widely applicate into human life and industry as a kind of energy storage system. However, the lacks of lithium natural source and increasing cost have limited the further development of LIBs, which arise the demand for developing some alternatives to LIBs. Comparing with LIBs, sodium ion batteries (SIBs) possess the advantages of the more abundant natural source of sodium and lower cost, which make it more promising for future application.[1-4] Thus, SIBs have attracted increasing attention in recent years. To date, most researches on SIBs are concentrated on cathode materials, while the investigation about anode materials is relatively less.

Recently, tuning crystallographic structure of oxides to improve the diffusion and transport of electrolyte ions have become a hot research topic.[5-12] Transition metal oxides have been traditionally used as anode materials for LIBs and SIBs, such as TiO_2, [13-16] Fe_3O_4, [17,18] CuO, [19,20] $NiCo_2O_4$.[21,22] Among various transition metal oxides, manganese oxide have attracted a great many attention for their different oxidation states of manganese, the low toxicity, the low cost, and superior safety.[23-25] As investigated in LIBs, manganese dioxide owns a high theoretical specific capacity of ~1230 mAh g^{-1}, and possesses relatively low electrochemical motivation force compared with other transition metal oxides.[26,27]

However, to date, there are few reports about the application of MnO_2 as anode materials for SIBs. This may be attributed to its shortages, such as aggregation, the volume expansion, and poor electronic conductivity, which resulted in the rapid irreversible fading of capacities following the cycling process. Meanwhile, it was proved that nanostructured MnO_2 materials could achieve better electrochemical performance. For instance, space-confined MnO_2 nanocrystallites exhibited an initial discharge capacity of 567 mAh g^{-1}.[28] Zhang et al reported that MnO_2 nanorods and nanoflowers could deliver an initial specific capacity of 427 and 488 mAh g^{-1}, respectively.[29] Besides, binder additives also have a negative influence on the conductivity of electrode and further electrochemical performance. In fact, many researchers have attempted to apply binder-free materials on LIBs and SIBs by using different substrates such as Ti foam, Ni foam, carbon cloth et al. [30-32]

Herein, we reported a unique feather-like MnO_2 nanostructure in-situ grown on a carbon paper (CP) via a simple hydrothermal method and its excellent electrochemical performance as a negative electrode for SIBs for the first time. The formation mechanism of the feather-like MnO_2 nanostructure on CP was investigated in detail. Moreover, the storage mechanism of sodium ions and the relationship between the structure and electrochemical properties were also investigated in this work.

Results and Discussion

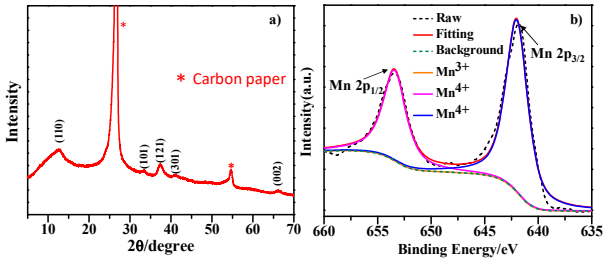

Figure 1. (a) XRD pattern and (b) XPS spectrum for Mn2p of the feather-like MnO_2 on CP.

[a] H. Li, Z. L. Guo, N. N. Wang, T. L. Ma
Graduate School of Life Science and Systems Engineering
Kyushu Institute of Technology
2-4 Hibikino, Wakamatsu, Kitakyushu, Japan
E-mail: tinglima@life.kyutech.ac.jp
[b] A. M Liu
School of Petroleum and Chemical Engineering
Dalian University of Technology
Liaoning, 124221, China
[c] S. Zhao
School of Science
Chongqing University of Technology
Chongqing, 400054, China

Supporting information for this article is given via a link at the end of the document.

The XRD analysis was applied to confirm the phase of the as-prepared sample. As depicted in Figure 1a, all the peaks could be indexed to the standard PDF card of α-MnO_2 (JCPDs No.01-072-1982) except for the peaks of the CP substrate. The diffraction peaks at 12.7°, 32.7°, 37.6°, 42.0°, 65.5° correspond to the (110), (101), (121), (301), (002) face of α-MnO_2 (Space group: I4/m), respectively. As a comparison, the XRD pattern of carbon paper was also displayed in Figure S1.

The XPS spectrum of Mn2p displayed in Figure 1b was used to investigate the valance state of Mn in the MnO_2 on CP. From Figure 1b, two peaks located at 642.1 and 653.7 eV assigned to Mn $2p_{3/2}$ and Mn $2p_{1/2}$, respectively, can be observed. The peak value was consistent with other reports about MnO_2, indicating the actually 4^+ oxidation state of Mn.[33,34] Thus, the MnO_2 was successfully grown on carbon paper.

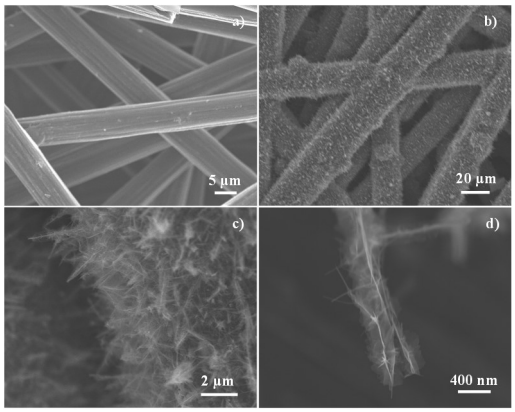

Figure 2. SEM images of (a) carbon paper substrate and (b-d) the feather-like MnO_2 on CP.

Figure 2 shows the SEM images of the carbon paper and as-prepared MnO_2/CP sample. The initial CP was composed of many carbon microfibers with a relatively smooth surface and a uniform diameter of ca. 15 μm, as shown in Figure 2a. From Figure 2b, it can be obviously observed that the CP was uniformly coated by the as-prepared MnO_2. The MnO_2 grown on CP exhibited a feather-like structure composed of many ultrathin nanowires. The rachis of the feather with over 2 μm in length connected with the carbon microfiber. Ultrathin nanowires were grown around the rachis just like barbs, which were about 10~15 nm in diameter.

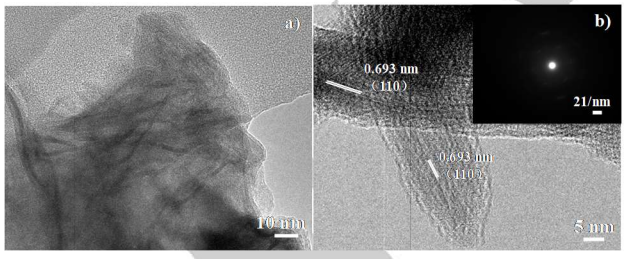

Figure 3. (a) TEM and (b) HRTEM images of the feather-like MnO_2 on CP.

In order to further investigate the detailed analysis of the samples, the morphology and structure were characterized by TEM and SAED. As shown in Figure 3a, several nanowires like the rachis of the feather could be observed. A lattice fringe of 0.693 nm could be observed from the HRTEM image in Figure 3b, which is assigned to the (110) facet of the α-MnO_2 phase. The inset in Figure 3b shows the SAED pattern of the feather-like MnO_2. Two multiple diffraction rings could be observed, indicating that the feather-like MnO_2 are polycrystalline.

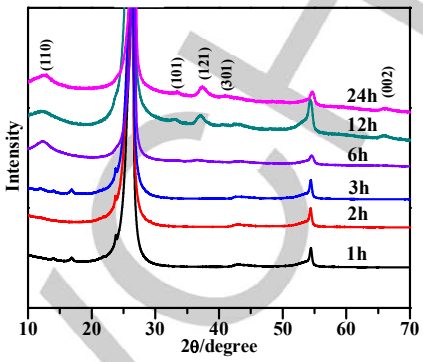

Figure 4. XRD patterns for the feather-like MnO_2 on CP with different reaction time.

In order to investigate the formation mechanism of the unique feather-like MnO_2 on CP, the samples with different reaction time were prepared. The XRD patterns of the as-prepared MnO_2 on CP with different reaction time were displayed in Figure 4. From 1 h to 6 h, only the diffraction peaks of CP could be observed and no peak of MnO_2 existed. When the reaction time prolonged to 12 h, the diffraction peaks of α-MnO_2 appeared. Furthermore, the sample obtained with 24 h reaction displayed stronger peak intensities.

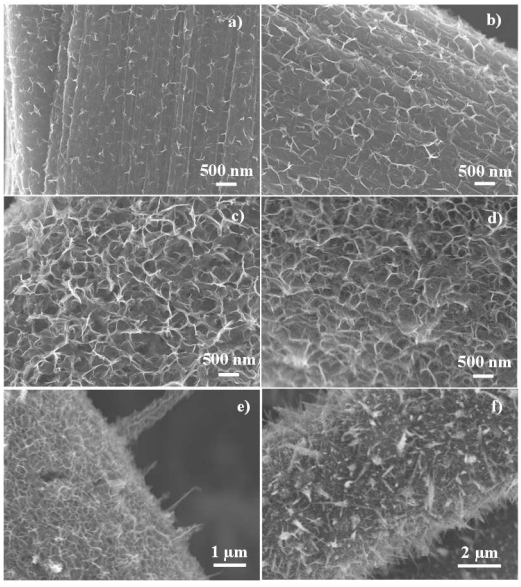

Figure 5. SEM images of feather-like MnO_2 on CP for different reaction time: (a) 1h, (b) 2h, (c) 3h, (d) 6h, (e) 8h and (f) 12h.

Moreover, the formation process of the feather-like MnO_2 grown on CP was also performed by SEM images with different reaction time (Figure 5). When the reaction time was increased from 1 h to 6 h, the surface of microfibers was slowly oxidized by $KMnO_4$ and changed to network morphology. When the reaction time increased to 6 h, the surface of microfibers was fully changed to the network structure. After reacting for 8 h, the feather-like MnO_2 was gradually grown on the surface of oxidized carbon microfibers. When reacting for 24 h, the carbon microfibers were uniformly coated by feather-like MnO_2.

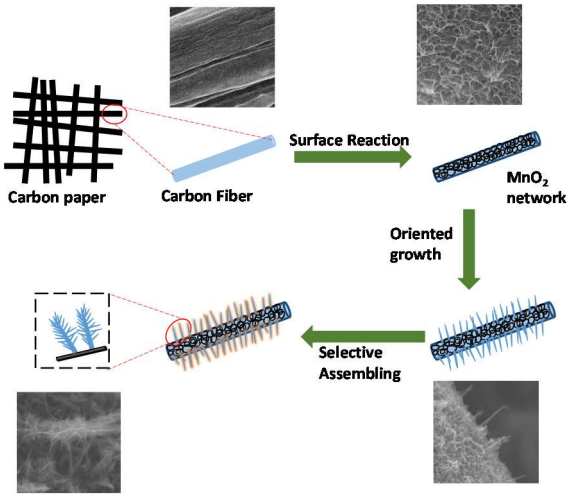

Scheme 1. Schematic illustration of the preparation of the feather-like MnO_2 on the CP.

The chemical reaction equations for the feather-like MnO_2 formation on the CP could be described as below: [33]

$$4MnO_4^- + 3C + H_2O \rightarrow 4MnO_2 + 2HCO_3^- + CO_3^{2-} \quad (1)$$

$$4MnO_4^- + 2H_2O \rightarrow 4MnO_2 + 4OH^- + 3O_2 \quad (2)$$

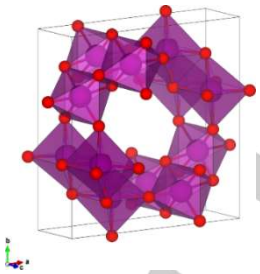

Figure 6. Crystal structure of α-MnO_2. Large (purple) octahedral represent approximate MnO_6 octahedral while Small (red) spheres represent oxygen.

According to above results and equations, a schematic process of preparing the feather-like MnO_2 on CP was proposed, as depicted in Scheme 1. Firstly, the CP was gradually reacted with MnO_4^-, resulting to the rougher surface of CP. When the reaction time was further prolonged, eqn (2) occurred and 1D MnO_2 nanowires began to grow on the rougher surface. With the increased time, ultrathin nanowires further grew on the 1D nanowires until the carbon fibers were all coated by uniformly feather-like nanostructure of MnO_2.

The crystal structure of α-MnO_2 was shown in Figure 6. In a typical unit cell of α-MnO_2, along the c-axis direction both corner-sharing and edge-sharing approximate MnO_6 octahedra exists to form a 2 × 2 tunnel structure. Then all of the MnO_6 octahedra are connected by edge-sharing to form a densely packed wall to the tunnel, parallel to the c-axis. The open tunnel structure of α-MnO_2 makes it an ideal candidate for sodium ion insertion.

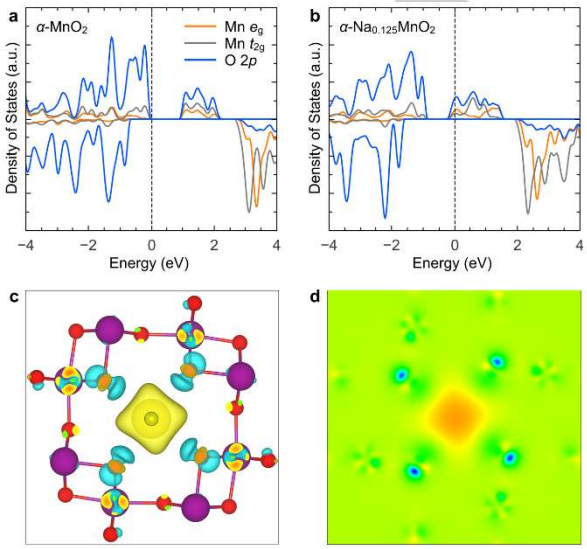

Figure 7. Calculated PDOS for (a) the *α*-MnO_2 and (b) *α*-$Na_{0.125}MnO_2$ by PBE+U method. The differential charge density of the Na intercalation in the *α*-MnO_2 (c) and a slice along the (001) plane (d).

Table 1. Optimized and experimental lattice parameters for α-MnO_2.

	a(Å)	b(Å)	c(Å)	α, β, γ (deg)
PBE+U	9.732	9.732	2.928	90
Expt.	9.750	9.750	2.861	90

The lattice parameters presented in Table 1 was optimized by the PBE+U method. We can see that the optimized values are well in agreement with the experimental results. To study the electronic properties of α-MnO_2, the partial density of states (PDOS) based on the optimized crystal structure were calculated, as shown in Figure 7. It is clear that the α-MnO_2 shows semiconductor characteristic. In the spin-up channel, the upper valence bands consist mainly consisted of the O 2p and Mn t_{2g} states, and the lower conduction bands are composed of the hybridization of Mn 3d and O 2p states. In the spin-down channel, a much broader band gap was found near the Fermi energy level. In this case, the upper valence bands predominantly consisted of the occupied O 2p states, and the lower conduction bands are formed by the unoccupied Mn 3d states. In α-MnO_2, the Mn is supposed to be +4 state with the electronic configure of $3t_{2g}^3e_g^0$. However, due to the localized feature of 3d electrons, the eg state of Mn can also be found at the valence bands. When Na inserted into the α-MnO_2, the Fermi energy level increased due to the additional electron. The hybridization of Mn 3d and O 2p states crosses the Fermi energy level in the spin-up channel of α-$Na_{0.125}MnO_2$, resulting into the electronic conductivity. The charge redistribution caused by the Na intercalation can be studied by calculating the differential charge density, which is shown in Figure 7. We can see that the inserted Na donates charge to the neighboring O anions as well as the Mn cations. The shape of the

differential charge suggests that the additional electrons reorganize onto the O 2p and Mn 3d states, which is consistent with the PDOS results.

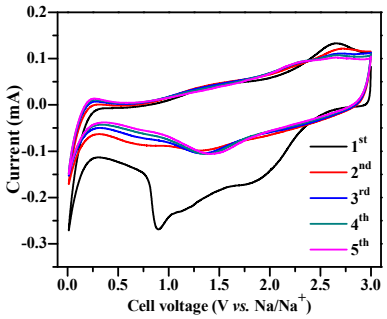

Figure 8. CV curves for the initial five cycles at a scan rate of 0.5 mV s^{-1} of the feather-like MnO_2/CP electrode.

The hierarchical feather-like structure makes it a promising material as anode for SIBs. The CV curves of as-prepared MnO_2 on CP were shown in Figure 8. The reduction process for the 1st cycle was different with the subsequent 4 cycles, which might due to the formation of solid electrolyte interphase (SEI) film in the electrolyte surface and some irreversible structural changes in the 1st cycle. [28] A redox peak at 0.9 V observed for the 1st cycle could be attributed to the electrochemical reaction of carbon paper, which was consistent with the CV curves of pure carbon paper in Figure S2. Meanwhile, for the subsequent cycles, the CV curves demonstrated the carbon paper substrate had nearly no contribution on the electrochemical performance. In the subsequent cycles, only a redox peak at 1.4 V could be found while no oxidation peak was observed, which indicate the MnO_2 on CP may possess pseudocapacitive property.[40] Meanwhile, the position of anodic and cathodic peaks for each cycle did not change, indicating the reversibility of sodium ion storage process in the MnO_2 on CP electrode.

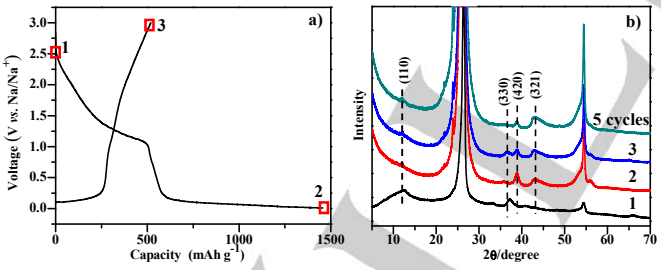

Figure 9. (a) Charge-discharge profiles and (b) corresponding XRD patterns for the 1st cycle of the feather-like MnO_2/CP electrode.

Figure 9a shows the charge-discharge profiles for the initial cycle under a current density of 0.05 A g^{-1}. In the initial cycle, the MnO_2/CP electrode exhibited a discharge specific capacity as high as 1456.0 mAh g^{-1} while the charge capacity was 519.1 mAh g^{-1}. The low Coulombic efficiency for the 1st cycle may be resulted by the formation of solid electrolyte interphase (SEI) film in the initial cycle, which in agreement with the results of CV profiles. To investigate the sodium insertion mechanism and structural change of MnO_2 active materials in the initial cycle, the XRD patterns for the MnO_2 on CP at different voltages were carried out. Interestingly, when the cell firstly discharged to 0.01V, the diffraction peaks shifted to 12.1°, 37.0°, 39.0° and 44.8°, corresponding to the (110), (330), (420) and (321) face of α-MnO_2 (JCPDs card No.00-053-0633). For the following charging process and cycles, the diffraction peaks did not change. This shift of diffraction peaks might be due to the insertion of Na^+ into the tunnel structure of MnO_2, leading to the occurrence of in-situ topotactic transition reaction. [35] This result also indicated the good stability of the as-prepared feather-like MnO_2 on CP after the electrochemical reaction.

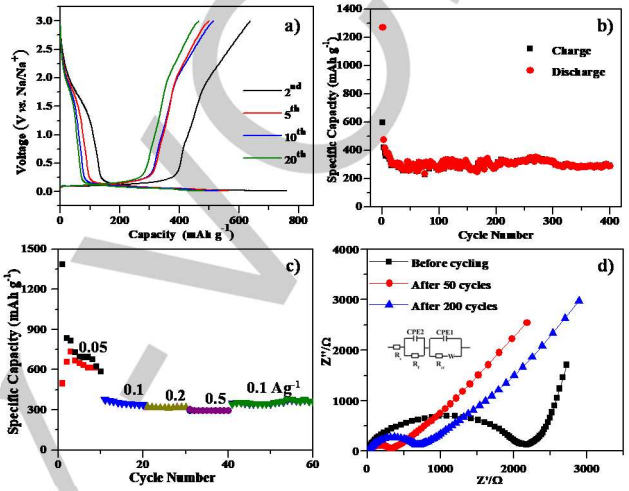

Figure 10. (a) Charge-discharge profiles for the 2nd, 5th and 20th cycles at a current density of 0.05 A g^{-1}, (b) cycling performance at a current density of 0.1 A g^{-1}, (c) rate performance at different current densities and (d) EIS plots before and after cycling of the feather-like MnO_2/CP electrode.

Figure 10a shows the charge-discharge profiles of the MnO_2 on CP electrode for the 2nd, 5th, 10th and 20th cycle under a current rate of 0.05 A g^{-1}. A discharge capacity of 760.8, 563.4, 532.2 and 487.1 mAh g^{-1} could be delivered at the 2nd, 5th, 10th and 20th cycle, respectively. The increased Coulombic efficiency indicated the excellent reversibility of feather-like MnO_2 on CP. The long cycling performance of the feather-like MnO_2 on CP electrode was also measured with a rate of 0.1 A g^{-1}. As presented in Figure 10b, after cycling for even 400 times the MnO_2 on CP could still exhibit a high discharge capacity of ~300 mAh g^{-1} and remain a capacity retention of 63% based on the 2nd cycle, illustrating the excellent cycling stability of the electrode. Figure 10c shows the rate performance of the MnO_2 on CP from 0.05 to 0.5 A g^{-1}. The electrode exhibited a specific capacity of 835.8, 379.5, 323.2 and 305.60 mAh g^{-1} under different current densities of 0.05, 0.1, 0.2 and 0.5 A g^{-1}, respectively. Besides, a high discharge capacity of 341.6 mAh g^{-1} could be remained when returned to the current rate of 0.1 A g^{-1} after 40 cycles. The rate performance demonstrated that the feather-like MnO_2 nanostructure on CP possesses excellent rate capability and stability.

The EIS plots of the MnO_2 on CP electrode without cycling and with 50 cycles and 200 cycles were presented in Figure 10d. The EIS plots were all consisted of a semicircle at high frequency regions and an inclined straight line in low frequencies. The semicircle at high frequencies corresponded to the charge transfer resistance and Ohmic resistance. Besides, the short inclined line could be related to the diffusion rate of sodium ions

within the anode electrode. As depicted in the fitted equivalent circuit model inset of Figure 10d, the circuit model was composed of the electrolyte resistance R_s, the SEI resistance R_f, the charge-transfer resistance R_{ct}, two constant phase elements (CPE1 and CPE2) related to the charge-transfer resistance and interfacial resistance and the Warburg impedance (W) which corresponded to the diffusion rate of Na ions during electrochemical process. Obviously, the charge transfer resistance after cycling for 50 times was lower than before, which is consistent with the calculation results that the MnO_2 on CP had been changed to a conductor characteristic from a semiconductor characteristic. When further cycling to 200 cycles, the semicircle becomes larger than that of 50 cycles, indicating the charge transfer resistance was increased. This might be a reason that the capacity of feather-like MnO_2 on CP decreased gradually with increasing cycling number.

Overall, the unique feather-like MnO_2 nanostructure on CP exhibited excellent sodium storage properties and reversibility. The 3D structure of carbon paper substrate could permit facile diffusion of the electrolyte inside the active material to enhance the transport of Na-ion and electron through the electrode film. On the other hand, the unique feather-like structure with a high surface area can be beneficial to increase the contact with the electrolyte and active mass to shorten the transportation distance of sodium ion and electron. Furthermore, using the MnO_2 on CP directly as an electrode can also eliminate the effects of the binder. Above all, the unique feather-like MnO_2 on CP anode exhibited excellent electrochemical properties.

Conclusions

In summary, a simple and facile hydrothermal method was used to prepare the unique feather-like MnO_2 on CP substrate for the first time. Furthermore, the MnO_2 on CP was employed as anode for SIBs and delivered high discharge capacities and excellent stability. A high capacity of ~300 mAh g^{-1} could be obtained even after cycling for 400 times at a current density of 0.1 A g^{-1}. The excellent electrochemical performance of feather-like MnO_2 on CP could be attributed to the unique feather-like structure and the network structure of carbon paper, which could shorten the lithium ion and electron transportation distance and promote the fast diffusion of electrolyte into the active materials. Therefore, the application of carbon paper could lead to advances for next-generation binder-free SIBs.

Experimental Section

Preparation of the feather-like MnO_2 on CP

The feather-like MnO_2 grown on CP was obtained by a simple one-step hydrothermal route. In a typical process, 0.03 g $KMnO_4$ was dissolved into 40 ml of deionized water and stirred for 30 min in a beaker. Then the homogeneous solution was transferred into a 50 ml Teflon stainless autoclave with a piece of carbon paper (5 cm × 2 cm), and further heated at 160 °C for 24 h. After cooling down to room temperature, the carbon paper was taken out from the autoclave and washed with deionized water for several times. Furthermore, the carbon paper was dried in an oven at 70 °C overnight.

Structural Characterization

X-ray diffraction (XRD) patterns of as-prepared samples were recorded on a PANalytical X'Pert spectrometer using Cu Kα radiation (λ=1.54056Å). The morphology and structure of the as-prepared samples were characterized by field-emission scanning electron microscopy (FE-SEM, JEOL JSM-6701F instrument) and transmission electron microscopy (TEM, JEOL JEM-2100F). A Shimadzu AXIS-His instrument was employed to carry out X-ray photoelectron spectroscopy (XPS) characterization for determining the valance of Mn element in MnO_2.

Computational methods

The density functional theory (DFT) calculations were carried out by Quantum ESPRESSO package.[37] The calculations have been implemented based on the generalized gradient approximation (GGA) with Perdew-Burke-Ernzerhof (PBE) exchange correlation functional.[38] Due to the strong localizeion feature of Mn 3d electrons, we performed the on-site Coulomb interaction calculation with the Ueff(Mn) = 4 eV, respectively.[39] A plane wave cutoff of 40 Ry was applied for the expansion of the wave functions, and the 2 × 2 × 6 k-mesh grid was employed for sampling the Brillouin zone.[40]

Electrochemical Measurements

The electrochemical performance of electrode materials was measured in the form of CR-2032 coin cells. The carbon paper was cut into small uniform sheets with a diameter of 10 mm and used directly as a working electrode. The loading mass of the MnO_2 materials in each disc was about 2 mg cm^{-2}. Sodium metal was used as a counter electrode. The electrolyte was 1 M $NaClO_4$ dissolved into a 1:1 mixed solution of the propylene carbonate (PC) solvent and ethylene carbonate (EC). 5% fluoroethylene carbonate (FEC) was applied as an additive in the electrolyte, and the glass microfiber membrane (Whatman GD/F) was employed as separators. A Land CT 2001A battery tester system was applied to measure the Galvanostatic charge/discharge tests at room temperature. Charge-discharge profiles were measured with a potential range of 0.01-3 V (vs. Na/Na^+) under different current densities. Besides, a CHI 760E electrochemical workstation was applied to carry out the cyclic voltammetry (CV) measurements from 0.01-3 V (vs. Na/Na^+) at a scan rate of 0.5 mV s^{-1} as well as the electrochemical impedance spectroscopy (EIS) measurements over a frequency range from 0.01 Hz to 100 kHz.

Acknowledgements

This work was supported by the Grant-in-Aid for Scientific Research (KAKENHI) program, Japan (C, Grant Number 15K05597) and Takahashi Industrial and Economic Research Foundation (Takahashi Grant Number 06-003-154).

Keywords: sodium ion batteries • MnO_2 • feather-like nanostructure • anode

[1] M. D. Slater, D. Kim, E. Lee, M. M. Doeff, C. S. Johnson, *Adv. Funct. Mater.* **2013,** *23,* 947;
[2] H. Pan, Y. Hu, L. Chen, *Energy & Environ. Sci.* **2013,** 6, 2338-2360.
[3] C. Nithya, S. Gopukumar, *Wiley Interdisciplinary Reviews: Energy and Environment* **2015,** *4,* 253-278.
[4] M. Lao, Y. Zhang, W. Luo, Q. Yan, W. Sun, S. X. Dou, *Adv. Mater.* **2017,** 1700622.
[5] M. Guignard, C. Didier, J. Darriet, P. Bordet, E. Elkaim, C. Delmas, Nat. Mater. **2013,** *12,* 74-80.
[6] D. Kundu, B. Adams, V. Duffort, S. Vajargah, L. Nazar, Nat. Energy **2016,** *1(10),* 16119.
[7] B. Liu, X. Shi, X. Lang, L. Gu, Z. Wen, M. Zhao, Q. Jiang, Nat. Commun. **2018,** *9,*1375.

[8] Y. Yuan, C. Zhan, K. He, H. Chen, W. Yao, S. Sharifi-Asl, B. Song, Z. Yang, A. Nie, X. Luo, H. Wang, S. Wood, K. Amine, M. Islam, J. Lu, R. Yassar, Nat. Commun. **2016,** *7,*13374.

[9] Z. Li, K. Xiang, W. Xing, Wc Carter, Y. Chiang, Adv. Energy Mater. **2015,** *5,* 1401410.

[10] Y. Li, X. Shi, S. Lang, Z. Wen, J. Li, Q. Jiang, Adv. Funct. Mater. **2016,** *26,* 1830-1839.

[11] Y. Li, J. Li, X. Lang, Z. Wen, W. Zheng, Q. Jiang, Adv. Funct. Mater. **2017,** *27,* 1700447.

[12] G. Gautam, P. Canepa, W. Richards, R. Malik, G. Ceder, Nano Lett. **2016,** *16,* 2426-2431.

[13] Z. S. Hong, M. L. Kang, X. H. Chen, K. Q. Zhou, Z. G. Huang, M. D. Wei, *ACS Appl. Mater. Interfaces* **2017,** *9 (37),* 32071–32079.

[14] H. Li, Z. Zhang, X. Huang, T. B. Lan, M. D. Wei, T. L. Ma, *J. Energy. Chem.* **2017,** *26,* 667–672.

[15] M. Zhou, Y. Xu, C. L. Wang, Q. W. Li, J. X. Xiang, L. Y. Liang, M. H. Wu, H. P. Zhao, Y. Lei, *Nano Energy* **2017,** *31,* 514-524.

[16] J. F. Ni, S. D. Fu, C. Wu, J. Maier, Y. Yu, L. Li, *Adv. Mater.* **2016,** *28,* 2259–2265.

[17] J. Liu, X. Xu, R. Hu, L. Yang, M. Zhu, *Adv. Energy. Mater.* **2016,** *6(13).*

[18] B. H. Hou, Y. Y. Wang, J. Z. Guo, Y. Zhang, Q. L.Ning, Y. Yang, W. H. Li, J. P. Zhang, X. L. Wang, X. L. Wu, *ACS Appl. Mater. Interfaces* **2018,** *10(4),* 3581–3589.

[19] L. J. Wang, K. Zhang, Z. Hu, W. C. Duan, F. Y. Cheng, J. Chen, *Nano Res.* **2014,** *7(2),* 199–208.

[20] S. Yuan, X. L. Huang, D. L. Ma, H. G. Wang, F. Z. Meng, X. B. Zhang, *Adv. Mater.* **2014,** *26,* 2273–2279.

[21] X. Q. Zhang, Y. C. Zhao, C. G. Wang, X. Li, J. D. Liu, G. H. Yue, Z. D. Zhou, *J. Mater. Sci.* **2016,** *51,* 9296–9305.

[22] A. K. Mondal, D. W. Su, S. Q. Chen, S. Q. Chen, K. Kretschmer, X. Q. Xie, H. Ahn, G. X. Wang, *ChemPhysChem* **2015,** *16,* 169-175.

[23] M. M. Thackeray, *Prog. Solid State Chem.* **1997,** *25,* 1−71.

[24] A. R. Armstrong, M. Holzapfel, P. Novak, C. S. Johnson, S. H. Kang, M. M. Thackeray,P. G. Bruce, *J. Am. Chem. Soc.* **2006,** *128,* 8694−8698.

[25] D. A. Tompsett, M. S. Islam, *Chem. Mater.* **2013,** *25,* 2515−2526.

[26] H. Lai, J. Li, Z. Chen, Z. Huang, *ACS Appl. Mater. Interfaces* **2012,** *4,* 2325.

[27] L. Li, A. O. Raji, J. M. Tour, *Adv. Mater.* **2013,** *25,* 6298–6302.

[28] Y. Weng, T. Huang, C. Lim, P. Shao, S. Hy, C. Kuo, J. Cheng, B. J. Hwang, J. Lee, N. Wu, *Nanoscale* **2015,** *7,* 20075-20081.

[29] Z. Zhang, X. X. Zhao, J. Li, *ChemNanoMat* **2016,** *2,*196-200.

[30] H. Li, H. Fei, X. Liu, J. Yang, M. Wei, *Chem. Commun.* **2015,** *51(45),* 9298-9300.

[31] T. Gu, Z. Cao, B. Wei, *Adv. Energy Mater.* **2017,** *7(18).*

[32] Y.Jin, H. Yuan, J. Lan, Y. Yu, Y. Lin, X. Yang, *Nanoscale* **2017,** *9(35),*13298-13304.

[33] V. Subramanian, H. W. Zhu, R. Vajtai, P. M. Ajayan, B. Q. Wei, *J. Phys. Chem. B* **2005,** *109,* 20207-20214.

[34] J. Yan, Z. J. Fan, T. Wei, W. Z. Qian, M. L. Zhang, F. Wei, *Carbon* **2010,** *48(13),* 3825-3833.

[35] D. C. Chen, D. Ding, X. X. Li, G. H. Walter, X. H. Xiong, M. S. El-Sayed, M. L. Liu, Chem. Mater. **2015,** *27,* 6608-6619.

[36] C. Reitz, C. Suchomski, D. Wang, H. Hahn, T. Brezesinski, *J. Mater. Chem. C* **2016,** *4,* 8889-8896.

[37] P. Giannozzi, S. Baroni, N. Bonini, M. Calandra, R. Car, C. Cavazzoni, D. Ceresoli, G. L. Chiarotti, M. Cococcioni, I. Dabo, A. Dal Corso, S. De Gironcoli, S. Fabris, G. Fratesi, R. Gebauer, U. Gerstmann, C. Gougoussis, A. Kokalj, M. Lazzeri, L. Martin-Samos, N. Marzari, F. Mauri, R. Mazzarello, S. Paolini, A. Pasquarello, L. Paulatto, C. Sbraccia, S. Scandolo, G. Sclauzero, A. P. Seitsonen, A. Smogunov, P. Umari, R. M. Wentzcovitch, *J. Phys. Condens. Matter* **2009,** *21(39),* 395502.

[38] J. P. Perdew, K. Burke, M. Ernzerhof, *Phys. Rev. Lett.* **1996,** 77, 3865.

[39] S. L. Dudarev, G. A. Botton, S. Y. Savrasov, C. J. Humphreys, A. P. Sutton, *Phys. Rev. B - Condens. Matter Mater. Phys.* **1998,** *57,* 1505.

[40] J. D. Pack, H. J. Monkhorst, *Phys. Rev. B - Condens. Matter Mater. Phys.* **1977,** *16,* 1748.

ARTICLE

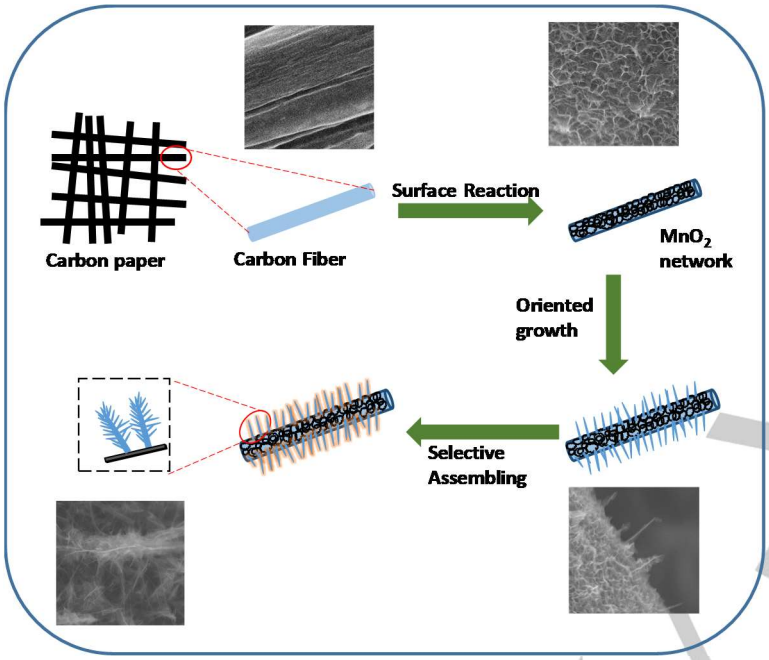

Caps off: The feather-like MnO_2 nanostructure was in-situ grown on carbon paper and delivered high performance as anode for sodium-ion batteries.

*Huan Li, Anmin Liu, Shuai Zhao, Zhanglin Guo, Nannan Wang, Prof. Tingli Ma**

Page No.1 – Page No.6

In-situ growth of a feather-like MnO_2 nanostructure on carbon paper for high performance rechargeable sodium-ion batteries